Remote Sensing of Environment 215 (2018) 1–6

Contents lists available at ScienceDirect

Remote Sensing of Environment

journal homepage: www.elsevier.com/locate/rse

Data synergy between leaf area index and clumping index Earth Observation products using photon recollision probability theory

Jan Pisek[a,*], Henning Buddenbaum[b], Fernando Camacho[c], Joachim Hill[b], Jennifer L.R. Jensen[d], Holger Lange[e], Zhili Liu[f], Arndt Piayda[g], Yonghua Qu[h], Olivier Roupsard[i], Shawn P. Serbin[j], Svein Solberg[e], Oliver Sonnentag[k], Anne Thimonier[l], Francesco Vuolo[m]

[a] Tartu Observatory, University of Tartu, 61602 Tõravere, Tartumaa, Estonia
[b] Environmental Remote Sensing & Geoinformatics, Faculty of Environmental and Regional Sciences, Trier University, D-54286 Trier, Germany
[c] EOLAB, Parc Científic Universitat de València, c/ Catedràtic José Beltrán, 2, 46980 Paterna, Valencia, Spain
[d] Department of Geography, Texas State University San Marcos, TX 7866, USA
[e] Norwegian Institute of Bioeconomy Research, Ås, Akershus, Norway
[f] Center for Ecological Research, Northeast Forestry University, Harbin 150040, China
[g] Thünen Institute of Climate-Smart Agriculture, Bundesallee 65, 38116 Braunschweig, Germany
[h] State Key Laboratory of Remote Sensing Science, Beijing Key Laboratory for Remote Sensing of Environment and Digital Cities, School of Geography, Beijing Normal University, Beijing 100875, China
[i] CIRAD-Persyst, UMR Ecologie Fonctionnelle and Biogéochimie des Sols et Agroécosystèmes, SupAgro-CIRAD-INRA-IRD, Montpellier, France
[j] Brookhaven National Laboratory, Environmental & Climate Sciences Department, Upton, NY 11973-5000, USA
[k] Département de géographie and Centre d'études nordiques, Université de Montréal, Montréal, QC H2V 2B8, Canada
[l] WSL-Swiss Federal Institute for Forest, Snow and Landscape Research, Zürcherstrasse 111, 8903 Birmensdorf, Switzerland
[m] Institute of Surveying, Remote Sensing and Land Information, Peter-Jordan-Straße 82, 1190 Vienna, Austria

ARTICLE INFO

Keywords:
Photon recollision probability
Foliage clumping index
Leaf area index
Multi-angle remote sensing

ABSTRACT

Clumping index (CI) is a measure of foliage aggregation relative to a random distribution of leaves in space. The CI can help with estimating fractions of sunlit and shaded leaves for a given leaf area index (LAI) value. Both the CI and LAI can be obtained from global Earth Observation data from sensors such as the Moderate Resolution Imaging Spectrometer (MODIS). Here, the synergy between a MODIS-based CI and a MODIS LAI product is examined using the theory of spectral invariants, also referred to as photon recollision probability ('*p*-theory'), along with raw LAI-2000/2200 Plant Canopy Analyzer data from 75 sites distributed across a range of plant functional types. The *p*-theory describes the probability (*p*-value) that a photon, having intercepted an element in the canopy, will recollide with another canopy element rather than escape the canopy. We show that empirically-based CI maps can be integrated with the MODIS LAI product. Our results indicate that it is feasible to derive approximate *p*-values for any location solely from Earth Observation data. This approximation is relevant for future applications of the photon recollision probability concept for global and local monitoring of vegetation using Earth Observation data.

1. Introduction

Clumping index (CI) is a measure of foliage aggregation relative to a random distribution of leaves in space (Nilson, 1971; Chen and Black, 1992). The CI is an important factor for the correct quantification of true leaf area index (LAI). The CI is also needed for estimating fractions of sunlit and shaded leaves in the canopy (Norman, 1982) - an effective way for upscaling from leaf to canopy for modeling vegetation photosynthesis (Bonan et al., 2014; He et al., 2017; Jiang and Ryu, 2016). Global and regional scale CI maps have been generated from various multi-angle sensors (e.g. He et al., 2012; Pisek et al., 2010, 2013a; Wei and Fang, 2016) based on an empirical relationship with the normalized difference between hotspot and darkspot (NDHD) index (Chen et al., 2005). Ryu et al. (2011) suggested that the adequate representation of canopy radiative transfer, important for the simulation of gross primary productivity and evapotranspiration (Baldocchi and Harley, 1995), is possible by integrating CI with incoming solar irradiance and LAI from Moderate Resolution Imaging Spectrometer (MODIS) land and atmosphere products. It should be noted that the MODIS LAI/FPAR product (MOD15A2H) uses internal a set of non-

* Corresponding author.
E-mail address: janpisek@gmail.com (J. Pisek).

https://doi.org/10.1016/j.rse.2018.05.026
Received 14 December 2017; Received in revised form 24 May 2018; Accepted 25 May 2018
Available online 30 May 2018
0034-4257/

empirical, stochastic equations for the parameterization of foliage clumping (Shabanov et al., 2003). Our objective is to find out if the MODIS LAI product with its non-empirical, stochastic clumping parameterization can be used together with empirically-based CI maps, e.g. for the calculation of sunlit/shaded fractions of LAI.

Here, we assess the synergy between a MODIS-based CI (He et al., 2012) and a MODIS LAI product (Yan et al., 2016a, 2016b) using the theory of spectral invariants or '*p*-theory' (Knyazikhin et al., 1998) along with raw LAI-2000/2200 Plant Canopy Analyzer (PCA; LI-COR Biosciences, Lincoln, NE, USA) data from 75 sites surveyed across a range of plant functional types (PFTs). The *p*-theory predicts that the amount of radiation scattered (reflected or transmitted) within a canopy depends only on the wavelength and the spectrally invariant canopy structural parameter *p*. It can be interpreted as the probability of a photon, having intercepted an element in the canopy, to recollide with another canopy element rather than escape the canopy (Smolander and Stenberg, 2005). The parameter *p* is linked to the foliage clumping (Stenberg et al., 2016). Simulation studies by Mõttus et al. (2007) and Smolander and Stenberg (2005) showed the recollision probability is closely related to LAI, with *p*-LAI relationships varying with the degree of clumping in the spatial distribution of leaf (needle) area. At a fixed LAI, *p*-value is larger the more aggregated the leaves in a canopy, or the smaller the canopy CI. The *p*-theory is intuitive and connected to the radiative transfer theory through the eigenvalues of the radiative transfer equation (Knyazikhin et al., 1998). Stenberg et al. (2016) provide an excellent review of the photon recollision probability concept in modeling the radiation regime of canopies.

2. Materials and methods

2.1. Method

Stenberg (2007) proposed to approximate a photon recollision probability for a canopy (*p*-value) from the Plant Canopy Analyzer (PCA) as:

$$p = 1 - (i_0/LAI_{true}) \quad (1)$$

where p is photon recollision probability, LAI_{true} is true leaf area index, and i_0 is canopy interceptance (the portion of the incoming radiation (photons) that is intercepted by the leaves), which can be expressed as:

$$i_0 = 1 - t_0 \quad (2)$$

where i_0 and t_0 are canopy interceptance and transmittance under diffuse, isotropic illumination conditions with constant directional intensity (Stenberg, 2007). Both i_0 and t_0 describe first interactions (with the canopy or the ground) only, and do not include photons which escape or interact again after being scattered from a leaf or the ground (Stenberg, pers. comm). Stenberg (2007) and Smolander and Stenberg (2005) further assume the canopy to have spherical leaf/shoot orientation and to be bounded underneath by a non-reflecting surface. t_0 is obtained as:

$$t_0 = 2\int_0^{\frac{\pi}{2}} \overline{cgf}(\theta)\sin(\theta)\cos(\theta)d\theta \quad (3)$$

where $\overline{cgf}$ is the canopy gap fraction at zenith angle θ (averaged over azimuth angle and horizontal area). Eqs. (1) and (2) can be combined to give:

$$p = 1 - \frac{1 - 2\int_0^{\frac{\pi}{2}} \overline{cgf}(\theta)\sin(\theta)\cos(\theta)d\theta}{LAI_{true}} \quad (4)$$

It should be noted that p as defined by Stenberg (2007) is a canopy structural characteristic which is independent of the above canopy radiation conditions. The PCA-based LAI estimate (LAI_{PCA}) is calculated here as the mean of the logarithms of the gap fraction values with clumping effects partially considered (Ryu et al., 2010):

$$LAI_{PCA} = -2\int_0^{\frac{\pi}{2}} \overline{\ln(cgf(\theta))}\sin(\theta)\cos(\theta)d\theta \quad (5)$$

For the coniferous sites, the PCA estimate (LAI_{PCA}) is further converted to true LAI using a shoot-scale grouping correction factor γ_E ($LAI_{true} = LAI_{PCA} * \gamma_E$) before calculating p (Rautiainen et al., 2009).

Alternatively, t_0 can be also estimated for an effective zenith angle θ as a function of LAI, mean projection of unit foliage area (G) (Ross, 1981), and clumping index (CI) (Chen et al., 2005):

$$t_0(\theta) = \exp[-G(\theta)CI\ LAI_{true}/\cos\theta] \quad (6)$$

Combining Eqs. (1) and (2) with (6), photon recollision probability p can then be calculated with CI and LAI estimated from Earth Observation data as:

$$p = 1 - (1 - \exp[-G(\theta)CI\ LAI_{true}/\cos\theta])/LAI_{true} \quad (7)$$

with $G(\theta) = 0.5$ and θ set as 57.3° to minimize the uncertainty about leaf angle orientation information (Pisek et al., 2013b) and assuming that t_0 in Eq. (2) for the upper hemisphere can be approximated by t_0 (57.3°). Eqs. (4) and (7) provide a simple way to evaluate the synergy of MODIS LAI (Yan et al., 2016a) and CI (He et al., 2012) products with independent PCA estimates. In case of needleleaf forests, Eq. (7) needs to be further modified when used in combination with the MODIS LAI product (LAI_{MODIS}):

$$p = 1 - (1 - \exp[-G(\theta)\ CI\ \gamma_E LAI_{MODIS}/\cos\theta])/(LAI_{MODIS}\gamma_E) \quad (8)$$

as vegetation clumping is not accounted for at the shoot scale in the original MODIS LAI product (Yan et al., 2016b).

2.2. MODIS LAI data

The current version of the MODIS LAI/FPAR product (MOD15A2H) is Collection 6 (C6) (Yan et al., 2016a). The main algorithm is based on look-up tables (LUTs) simulated from a three-dimensional radiative transfer (3D RT) model (Knyazikhin et al., 1999; Myneni et al., 2002). The algorithm finds the best LAI and FPAR estimates with biome-specific LUTs using daily land surface Bi-directional Reflectance Factors (BRFs) along with their uncertainties. A back-up empirical method utilizes relationships between the Normalized Difference Vegetation Index and LAI/FPAR to produce lower quality LAI estimates. The LAI value corresponding to the maximum FPAR is selected over the compositing period of four or eight days. Vegetation clumping in the 3D RT is accounted for at plant and canopy scales.

The most important improvement in MOD15A2H C6 compared to previous versions is the increase from 1 km to 500 m spatial resolution. In addition, a new version of MODIS surface reflectances (MOD09GA C6) is used to replace the previous 1 km intermediate dataset (MODAGAGG). In C6 the 1 km static land cover input is replaced with new multi-year MODIS land cover product (MCD12Q1) at 500 m resolution.

Only MODIS LAI retrievals produced with the main RT algorithm closest to the date of PCA measurements (see Section 2.4) were used in this study.

2.3. MODIS CI data

He et al. (2012) derived a global CI map at 500 m spatial resolution using the red band (620–670 nm) from the MODIS BRDF Model Parameters product (MCD43A1; Schaaf et al., 2002). Since MODIS does not observe near the hotspot and the angular kernels used to construct the MODIS BRDF product do not include the complete hotspot physics and consistently underestimate the hotspot, He et al. (2012) developed an approach to correct the MODIS hotspot magnitude with synchronous co-registered POLDER-3 data. After the MODIS hotspot correction, CI is derived using two coefficients calculated from the second-order polynomial fit of the tabulated relationship between CI and NDHD by Chen et al. (2005). He et al. (2012) assigned a single annual CI value, the

Table 1
Characteristics and results for 75 sites with raw PCA measurements. PFT is plant functional type. Lat is latitude (in degrees). Lon is longitude (in degrees). PCA is Plant Canopy Analyzer. LAI_{PCA} is LAI estimate from PCA data. p is the photon recollision probability. γ_E is the needle-to-shoot area ratio.

PFT	Country	Site name	Lat	Lon	Species	raw PCA data source	LAIPCA	t0	p	γ_E
CRO	Austria	Marchfeld_B	48.16N	16.7E	Beet	Vuolo et al. (2013)	2.87	0.095	0.72	
CRO	Austria	Marchfeld_M	48.18N	16.92E	Maize	Vuolo et al. (2013)	3.10	0.089	0.72	
CRO	Austria	Marchfeld_W	48.18N	16.91E	Wheat	Vuolo et al. (2013)	0.55	0.683	0.48	
CRO	China	Heilongjiang	48.13N	126.96E	Corn	Qu et al. (2016)	0.72	0.548	0.42	
CRO	Costa Rica	Aquiares	9.93N	83.71W	Coffee	Taugourdeau et al. (2014)	2.66	0.107	0.70	
CRO	Japan	Nagaoka	37.48N	138.78E	Rice – early planted	Kobayashi (unpublished)	2.72	0.124	0.70	
CRO	Japan	Nagaoka	37.48N	138.78E	Rice – later planted	Kobayashi (unpublished)	2.84	0.111	0.71	
CRO	Spain	Barrax C-3	39.06N	2.09W	Corn	Verger et al. (2009)	0.36	0.746	0.35	
CRO	Spain	Barrax C-2	39.05N	2.09W	Corn	Verger et al. (2009)	0.42	0.715	0.37	
DBF	Estonia	Järvselja	58.29N	27.26E	Silver birch	Kodar et al. (2008)	3.78	0.081	0.76	
DBF	Germany	Hohes Holz	52.08N	11.22E	Beech	Piayda (unpublished)	4.44	0.025	0.79	
DBF	Germany	Merzalben	49.26N	7.8E	Beech, oak	Pueschel et al. (2012)	4.24	0.029	0.77	
DBF	Italy	Ro1	42.41N	11.93E	Oak	Tedeschi et al. (2006)	3.70	0.052	0.75	
DBF	Italy	Ro2	42.39N	11.92E	Oak	Tedeschi et al. (2006)	4.57	0.028	0.79	
DBF	Japan	Takayama	36.14N	137.42E	Mongolian oak	Nasahara et al. (2008)	3.66	0.045	0.74	
DBF	Korea	Gwangneung	37.76N	127.15E	Oak	Kwon (unpublished)	4.57	0.018	0.79	
DBF	Switzerland	Bettlachstock	47.23N	7.41E	Beech	Thimonier et al. (2010)	4.53	0.02	0.79	
DBF	Switzerland	Isone	46.13N	9.01E	Beech	Thimonier et al. (2010)	3.81	0.035	0.76	
DBF	Switzerland	Lausanne	46.58N	6.66E	Beech	Thimonier et al. (2010)	5.45	0.012	0.82	
DBF	Switzerland	Neunkirch	47.68N	8.53E	Beech	Thimonier et al. (2010)	3.76	0.04	0.75	
DBF	Switzerland	Schänis	47.16N	9.06E	Beech	Thimonier et al. (2010)	4.07	0.03	0.76	
DBF	Switzerland	Novaggio	46.01N	8.83E	Oak	Thimonier et al. (2010)	3.21	0.059	0.72	
DBF	Switzerland	Jussy	46.23N	6.28E	Oak, hornbeam	Thimonier et al. (2010)	4.12	0.031	0.78	
DBF	USA	Chestnut	35.93N	84.45W	Chestnut	Heuer (unpublished)	3.53	0.052	0.73	
DBF	USA	Harvard	42.53N	72.17W	Oak	Urbanski et al. (2007)	4.69	0.022	0.79	
DBF	USA	Coweeta	35.05N	83.45W	Oak-hickory	Hwang et al. (2009)	5.51	0.03	0.83	
EBF	France	Puechabon	43.74N	3.6E	Oak	Rambal et al. (2003)	3.06	0.081	0.70	
EBF	Portugal	Coruche	39.13N	8.33W	Oak	Piayda et al. (2015)	0.73	0.559	0.49	
EBF	Thailand	Kog-Ma	18.8N	98.9E	Lithocarpus	Tanaka et al. (2008)	3.65	0.048	0.74	
ENF	Canada	Scotty Creek	61.31N	121.3W	Black spruce	Sonnentag (unpublished)	0.83	0.514	0.75	1.36
ENF	Canada	Thompson_1850	55.87N	98.47W	Black spruce	Serbin et al. (2009)	2.28	0.206	0.73	1.36
ENF	Canada	Thompson_1930	55.89N	98.51W	Black spruce	Serbin et al. (2009)	2.07	0.214	0.63	1.36
ENF	Canada	Campbell river	49.51N	124.9W	Douglas fir - young	Chen et al. (2006)	2.75	0.108	0.82	1.66
ENF	Estonia	Järvselja	58.3N	27.24E	Norway spruce	Kodar et al. (2008)	3.12	0.095	0.82	1.42
ENF	Estonia	Järvselja	58.3N	27.26E	Scots pine	Kodar et al. (2008)	2.51	0.156	0.80	1.7
ENF	Korea	Gwangneung	37.76N	127.16E	Korean pine	Kwon (unpublished)	4.44	0.021	0.76	1.21
ENF	Norway	Østmarka_1	59.81N	11.0E	Norway spruce	Solberg et al. (2009)	2.17	0.216	0.70	1.42
ENF	Norway	Østmarka_2	59.81N	10.99E	Norway spruce	Solberg et al. (2009)	1.17	0.488	0.87	1.42
ENF	Norway	Østmarka_3	59.82N	11.0E	Norway spruce	Solberg et al. (2009)	5.17	0.021	0.81	1.42
ENF	Norway	Østmarka_5	59.82N	11.02E	Norway spruce	Solberg et al. (2009)	3.26	0.09	0.81	1.42
ENF	Norway	Østmarka_6	59.82N	11.02E	Norway spruce	Solberg et al. (2009)	3.28	0.085	0.84	1.42
ENF	Norway	Østmarka_7	59.81N	11.02E	Norway spruce	Solberg et al. (2009)	4.07	0.05	0.80	1.42
ENF	Norway	Østmarka_8	59.83N	11.03E	Norway spruce	Solberg et al. (2009)	3.11	0.096	0.79	1.42
ENF	Norway	Østmarka_9	59.83N	11.01E	Norway spruce	Solberg et al. (2009)	2.88	0.117	0.80	1.42
ENF	Norway	Østmarka_6_2003	59.82N	11.02E	Norway spruce	Solberg et al. (2009)	3.15	0.104	0.87	1.42
ENF	Norway	Østmarka_3_2003	59.82N	11.0E	Norway spruce	Solberg et al. (2009)	5.27	0.019	0.68	1.42
ENF	Norway	Østmarka_2_2003	59.81N	10.99E	Norway spruce	Solberg et al. (2009)	0.95	0.561	0.78	1.42
ENF	Norway	Østmarka_1_2003	59.81N	11.0E	Norway spruce	Solberg et al. (2009)	2.13	0.219	0.75	1.42
ENF	Switzerland	Alptal	47.05N	8.71E	Norway spruce	Thimonier et al. (2010)	2.73	0.1	0.77	1.42
ENF	Switzerland	Chironico	46.45N	8.81E	Norway spruce	Thimonier et al. (2010)	2.60	0.109	0.72	1.42
ENF	Switzerland	Lens	46.26N	7.43E	Scots pine	Thimonier et al. (2010)	2.09	0.164	0.67	1.7
ENF	Switzerland	Visp	46.3N	7.86E	Scots pine	Thimonier et al. (2010)	1.58	0.248	0.78	1.7
ENF	Switzerland	Vordemwald	47.28N	7.88E	Silver fir	Thimonier et al. (2010)	3.64	0.05	0.79	1.91
ENF	USA	US-NC2	35.48N	76.4W	Loblolly pine	Noormets et al. (2010)	4.23	0.034	0.87	1.21
ENF	USA	Howland	45.21N	68.74W	Red spruce	Richardson (unpublished)	1.94	0.2	0.81	1.6
ENF	USA	SJ57	47.13N	116.18W	Cedar, spruce, larch, pine	Jensen et al. (2008)	2.18	0.175	0.65	1.01
ENF	USA	527	46.22N	116.79W	Fir, pine, spruce, larch	Jensen et al. (2008)	1.94	0.189	0.59	1.01
GRA	Canada	Sandhill	53.79N	104.62W	Sedges	Sonnentag et al. (2010)	1.10	0.459	0.54	
GRA	USA	Vaira	38.41N	120.95W	Annual grass	Ryu et al. (2010)	0.99	0.416	0.53	
GRA	USA	Sherman	38.04N	121.75W	Invasive weed	Sonnentag (unpublished)	0.61	0.641	0.48	
MF	Canada	Timins	48.21N	82.15W	Aspen, spruce, birch, fir	Chen et al. (2006)	3.50	0.068	0.80	1.36
MF	Canada	Thompson_1964	55.91N	98.38W	Spruce, pine, aspen, willow	Serbin et al. (2009)	1.55	0.305	0.65	1.36
MF	Canada	Thompson_1981	55.85N	98.85W	Willow, jack pine, aspen	Serbin et al. (2009)	1.35	0.352	0.62	1.36
MF	Canada	Thompson_1989_1	55.90N	98.95W	Willow, jack pine, aspen	Serbin et al. (2009)	0.91	0.489	0.58	1.36
MF	Canada	Thompson_1989_2	55.91N	98.97W	Willow, jack pine, aspen	Serbin et al. (2009)	0.91	0.489	0.58	1.36
MF	Canada	Thompson_1994	56.16N	96.71W	Willow, jack pine, aspen	Serbin et al. (2009)	0.68	0.578	0.53	1.36
MF	China	SB	47.19N	128.87E	Birch, larch, pine	Liu et al. (2016)	2.32	0.179	0.74	1.08
MF	China	SC	47.19N	128.89E	Pine, birch, beech, elm	Liu et al. (2016)	3.60	0.053	0.80	1.28
MF	China	KP	47.18N	128.88E	Pine, birch, larch	Liu et al. (2016)	3.23	0.086	0.79	1.46
MF	China	BK	47.18N	128.9E	Pine, birch, maple, tilia	Liu et al. (2016)	3.62	0.054	0.80	1.41
MF	Estonia	Järvselja	58.29N	27.25E	Birch, spruce	Kodar et al. (2008)	3.59	0.06	0.81	1.42
MF	USA	WPA	47.63N	122.29W	Fir, maple, cedar, hemlock	Richardson et al. (2009)	2.91	0.082	0.68	1.36
OSH	Canada	Mer Bleue	45.4N	75.5W	Shrub (peatland)	Talbot et al. (2014)	2.69	0.104	0.68	

(*continued on next page*)

Table 1 (*continued*)

PFT	Country	Site name	Lat	Lon	Species	raw PCA data source	LAIPCA	t0	*p*	γ_E
OSH	Canada	Thompson_2003	55.9N	98.18W	Wild rose, fireweed	Serbin et al. (2009)	0.48	0.671	0.41	
WSA	USA	Tonzi	38.43N	120.97W	Blue oak	Ryu et al. (2010)	0.68	0.583	0.47	

CRO: crop, DBF: deciduous broadleaf forest, EBF: evergreen broadleaf forest, ENF: evergreen needleleaf forest, GRA: grass, MF: mixed forest, OSH: open shrubland, WSA: woody savanna.

median from its noisy seasonal trajectory, to each pixel in the final map. This global CI map is provided using the same pixel grid and projection as the MODIS LAI product (Section 2.2).

2.4. Plant Canopy Analyzer data

Ryu et al. (2010) compiled raw PCA instrument data from 41 sites distributed across six plant functional types ranging from boreal to tropical ecoclimatic zones. PCA data from 34 sites from their synthesis data set were retained after assessing their suitability for our study (e.g. representativeness of the area at the scale of corresponding overlapping 500 m MODIS pixel footprint verified with Google Earth Engine (Gorelick et al., 2017); temporal overlap with MODIS LAI product) (Table 1). In addition to the retained sites from Ryu et al. (2010), PCA measurements from 41 additional sites were included in this study. The available raw PCA data were used to approximate *p*-value at each site using Eq. (4). The corresponding γ_E values for given coniferous species were obtained from literature and are provided in Table 1.

3. Results and discussion

The relationship between LAI and photon recollision probability *p* approximated with PCA data using Eq. (4) is shown in Fig. 1. The nature of the *p*-LAI_{PCA} relationship is different between evergreen needleleaf (ENF) and other PFTs due to the inclusion of the shoot-scale correction factor (Chen, 1996). Compared to Rautiainen et al. (2009), the *p*-values representing needleleaf stands with greater variety of tree species were more dispersed. Our results support the notion by Rautiainen et al. (2009) that establishing species-specific *p*-LAI_{PCA} functions would require further research on the role of shoot-scale (shoot level) clumping and its documented variability between species (e.g. Chen et al., 2006; Stenberg et al., 1999, 2001) on photon recollision probability.

Eq. (7) assumes that t_0 in Eq. (3) for the upper hemisphere can be approximated by t_0 (57.3°). A regression between the gap fraction from the fourth ring (47–58° from zenith) and t_0 obtained from all five rings (Eq. (3)) for all sites is shown in Fig. 2. The tight linear relationship close to the 1:1 line indicates that this ring alone (or 57.3° as its representative) is indeed a reasonable approximation for t_0 of the upper hemisphere, while simultaneously reducing the uncertainty introduced through an assumed leaf inclination angle distribution. It should be noted that previous research by Leblanc and Chen (2001) also found that the fourth ring itself provides a good approximation of LAI_{PCA} under both direct and diffuse light conditions.

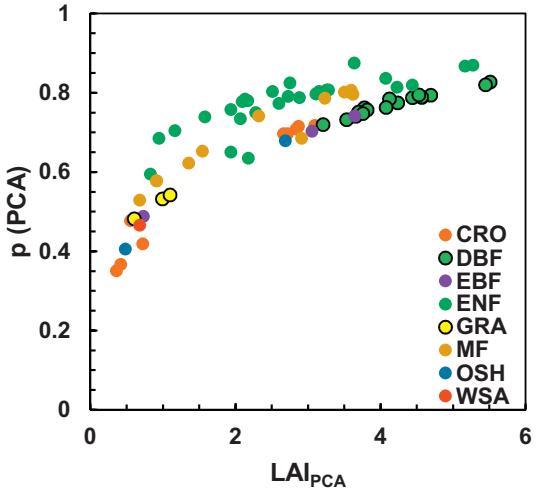

Fig. 1. Relationship between Plant Canopy Analyzer (PCA)-derived leaf area index (LAI_{PCA}) and approximated photon recollision probability *p*. The abbreviations used in the figure legend are explained in the caption of Table 1.

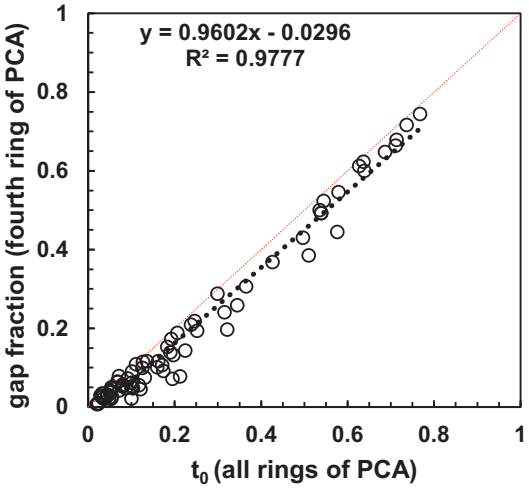

Fig. 2. Comparison between the transmittance (t_0; Eq. (3)) and gap fraction from the fourth ring of Plant Canopy Analyzer (PCA) data.

Fig. 3A shows a strong linear relationship (R^2 = 0.95; Mean Absolute Error (MAE) = 0.018; intercept 0.0043) between the *p*-values derived from Eqs. (4) and (7) using the PCA and γ_E data from Table 1 as the source of information about LAI, and CI values retrieved from He et al. (2012). Fig. 3A confirms the agreement between the two approaches (Eqs. (4) and (7)) to obtain *p*-value. The observed variation stems mainly from the uncertainty in G-function, CI values and approximation of t_0(57.3°) to t_0 of the upper hemisphere (Fig. 2). The clumping may change with season (Sprintsin et al., 2011; Pisek et al., 2015; Lang et al., 2017), while He et al. (2012) provide only the seasonal trajectory median value.

The linear relationship close to the 1:1 line (slope 1.0093; intercept −0.034) between the *p*-values derived from PCA and MODIS-only data (Fig. 3B) suggests a general compatibility of MODIS LAI and CI maps by He et al. (2012). Our results supports that a) the MODIS algorithm indeed uses the recollision probability to account for clumping, and b) the approach integrating the empirically based CI information with MODIS LAI suggested by Ryu et al. (2011) appears to be feasible. The difference between Fig. 3A and B is the inclusion of the MODIS LAI product in the latter one. Since the clumping in MODIS LAI is accounted for at the plant and canopy scales only, knowledge about the shoot-scale grouping correction factor γ_E is needed to retrieve the non-underestimated *p*-values in case of needleleaf forests.

Fig. 4 shows the scatterplot between LAI estimates from PCA and MODIS LAI C6 product. The increase in mean absolute error in Fig. 3B (MAE = 0.049) compared to Fig. 3A (MAE = 0.018) is linked to the

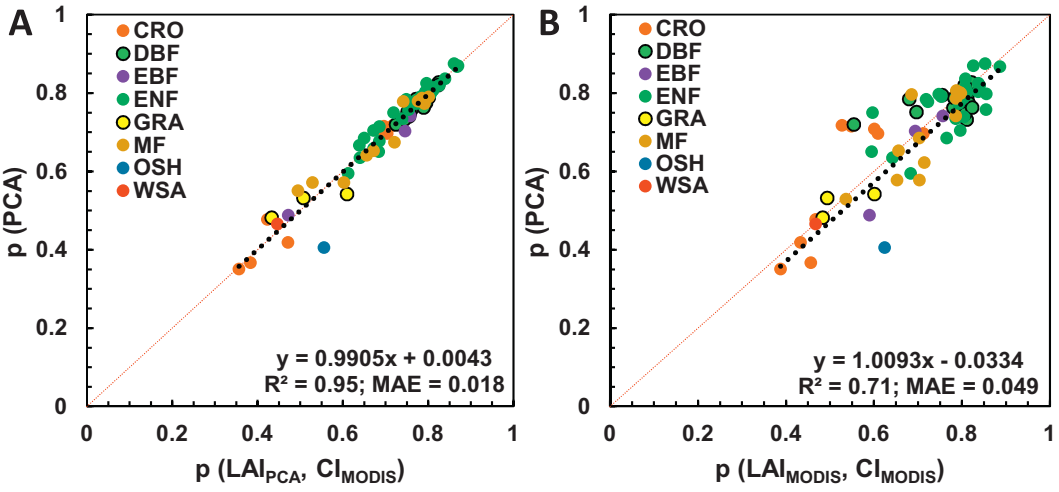

Fig. 3. Relationships between photon recollision probabilities *p* derived with Eqs. (4) and (7) using Plant Canopy Analyzer (PCA) data (A) and MODIS LAI C6 product (B) as LAI input into Eq. (7).

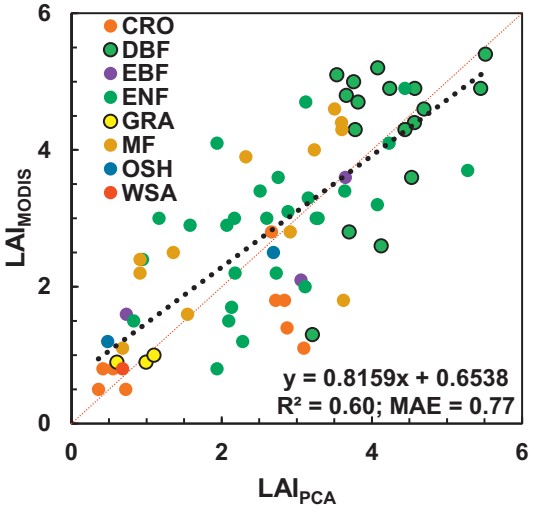

Fig. 4. Relationship between Plant Canopy Analyzer (PCA)-derived leaf area index (LAI_{PCA}) and MODIS LAI C6 product (LAI_{MODIS}). Both PCA and MODIS LAI data are not corrected for the shoot-scale grouping correction factor γ_E.

different estimates and sources of LAI information for Eq. (4) (PCA) and Eqs. (7) and (8) (MODIS LAI) as illustrated in Fig. 4. Furthermore, Fig. 1 shows that accurate LAI information for photon recollision probability estimation is particularly critical at lower LAI values. Since reflectance values are not saturated within LAI range of 0–2, LAI algorithms perform well within this domain (Yan et al., 2016b) and should be able to provide high quality input data. Importantly, it should be verified if the LAI input indeed corresponds to true LAI.

Our findings illustrate that it might be possible to obtain approximate *p*-values for any location solely from Earth Observation data, given availability of high quality LAI retrievals. In the future, the relationship could be possibly strengthened by further improved CI retrieval algorithms from Earth Observation data (e.g. Wei and Fang, 2016), by accounting for seasonal variation of clumping (He et al., 2016) and by knowing site specific G-function values (Raabe et al., 2015). It is envisioned that our findings provide a stimulus for future applications of the photon recollision probability concept for global and local monitoring of vegetation using Earth Observation data (Stenberg et al., 2016).

4. Conclusion

Our results indicate that the integration of a MODIS LAI product with empirically-based CI maps is feasible. Their synergy was assessed using the *p*-theory along with raw LAI-2000/2200 Plant Canopy Analyzer data gathered across a wide range of plant functional types. Importantly, for the first time it is shown that it might be possible to obtain approximate *p*-values for any location solely from Earth Observation data. This approximation is relevant for future applications of photon recollision probability concept for global and local monitoring of vegetation using Earth Observation data (Stenberg et al., 2016).

Acknowledgements

JP was supported by Estonian Research Council Grant PUT1355 and Mobilitas Pluss MOBERC11. The global clumping index map by He et al. (2012) is available for download through the following link: https://www.researchgate.net/publication/314151326_Global_Clumping_Index_Map. S.P.S. was partially supported by the United States Department of Energy contract No. DE-SC0012704 to Brookhaven National Laboratory.

The MODIS LAI C6 data have been accessed through Google Earth Engine. Dr. Youngryel Ryu kindly shared his compilation of raw PCA data. Original providers of the raw PCA data to Dr. Ryu are appreciated: Drs. Jing Ming Chen, Michael Gavazzi, Mark Heuer, Taehee Hwang, Joon Kim, Soo-Hyung Kim, Hideki Kobayashi, John Kochendorfer, Hyojung Kwon, Beverly Law, Craig Macfarlane, Francesco Mazzenga, Mark Mesarch, William Munger, Kenlo Nishida Nasahara, Asko Noormets, Jean-Marc Ourcival, Dario Papale, Serge Rambal, Andrew Richardson, Julie Talbot, Shashi Verma, and Leland Werden. Drs. Martin Béland, Yuri Knyazikhin, Philip Lewis and Pauline Stenberg provided valuable input and comments on the concept provided in this study. Authors wish to thank three anonymous reviewers for constructive comments on the manuscript.

References

Baldocchi, D.D., Harley, P.C., 1995. Scaling carbon dioxide and water vapour exchange from leaf to canopy in a deciduous forest. II. Model testing and application. Plant Cell Environ. 18, 1157–1173.

Bonan, G.B., Williams, M., Fisher, R.A., Oleson, K.W., 2014. Modeling stomatal conductance in the earth system: linking leaf water-use efficiency and water transport along the soil-plant-atmosphere continuum. Geosci. Model Dev. 7, 2193–2222. http://dx.doi.org/10.5194/gmd-7-2193-2014.

Chen, J.M., 1996. Optically-based methods for measuring seasonal variation of leaf area index in boreal conifer stands. Agric. For. Meteorol. 80, 135–163.

Chen, J.M., Black, T.A., 1992. Foliage area and architecture of plant canopies from sunfleck size distributions. Agric. For. Meteorol. 60, 249–266.
Chen, J.M., Menges, C.H., Leblanc, S.G., 2005. Global mapping of foliage clumping index using multi-angular satellite data. Remote Sens. Environ. 97, 447–457.
Chen, J.M., Govind, A., Sonnentag, O., Zhang, Y.Q., Barr, A., Amiro, B., 2006. Leaf area index measurements at Fluxnet-Canada forest sites. Agric. For. Meteorol. 140, 257–268.
Gorelick, N., Hancher, M., Dixon, M., Ilyushchenko, S., Thau, D., Moore, R., 2017. Google earth engine: planetary-scale geospatial analysis for everyone. Remote Sens. Environ. 202, 18–27.
He, L., Chen, J.M., Pisek, J., Schaaf, C.B., Strahler, A.H., 2012. Global clumping index map derived from the MODIS BRDF product. Remote Sens. Environ. 119, 118–130.
He, L., Liu, J., Chen, J.M., Croft, H., Wang, R., Sprintsin, M., Zheng, T., Ryu, Y., Pisek, J., Gonsamo, A., Deng, F., Zhang, Y., 2016. Inter- and intra-annual variations of clumping index derived from the MODIS BRDF product. Int. J. Appl. Earth Obs. Geoinf. 44, 53–60.
He, L., Chen, J.M., Croft, H., Gonsamo, A., Luo, X., Liu, J., ... Liu, Y., 2017. Nitrogen availability dampens the positive impacts of CO_2 fertilization on terrestrial ecosystem carbon and water cycles. Geophys. Res. Lett. 22, 11590–11600. http://dx.doi.org/10.1002/2017GL075981.
Hwang, T., Band, L.E., Hales, T.C., 2009. Ecosystem processes at the watershed scale: extending optimality theory from plot to catchment. Water Resour. Res. 45 (W11425). http://dx.doi.org/10.1029/2009WR007775.
Jensen, J.L.R., Humes, K.S., Vierling, L.A., Hudak, A.T., 2008. Discrete return lidar-based prediction of leaf area index in two conifer forests. Remote Sens. Environ. 112, 3947–3957.
Jiang, C., Ryu, Y., 2016. Multi-scale evaluation of global gross primary productivity and evapotranspiration products derived from Breathing Earth System Simulator (BESS). Remote Sens. Environ. 186, 528–547.
Knyazikhin, Y., Martonchik, J., Myneni, R., Diner, D., Running, S., 1998. Synergistic algorithm for estimating vegetation canopy leaf area index and fraction of absorbed photosynthetically active radiation from MODIS and MISR data. J. Geophys. Res. D103 (32) (257 – 32 276).
Knyazikhin, Y., Glassy, J., Privette, J.L., Tian, Y., Lotsch, A., Zhang, Y., Wang, Y., Morisette, J.T., Votava, P., Myneni, R.B., 1999. MODIS Leaf Area Index (LAI) and Fraction of Photosynthetically Active Radiation Absorbed by Vegetation (FPAR) Product (MOD15) Algorithm Theoretical Basis Document; Theoretical Basis Document. 1999. NASA Goddard Space Flight Center, Greenbelt, MD, USA, pp. 20771.
Kodar, A., Kutsar, R., Lang, M., Lukk, T., Nilson, T., 2008. Leaf area indices of forest canopies from optical measurements. Balt. For. 14 (2), 185–194.
Lang, M., Nilson, T., Kuusk, A., Pisek, J., Korhonen, L., Uri, V., 2017. Digital photography for tracking the phenology of an evergreen conifer stand. Agric. For. Meteorol. 246, 15–21.
Leblanc, S.G., Chen, J.M., 2001. A practical scheme for correcting multiple scattering effects on optical LAI measurements. Agric. For. Meteorol. 110, 125–139.
Liu, Z., Jin, G., Zhou, M., 2016. Evaluation and correction of optically derived leaf area index in different temperate forests. iForest-Biogeosciences and Forestry 9, 55–62.
Mõttus, M., Stenberg, P., Rautiainen, M., 2007. Photon recollision probability in heterogeneous forest canopies: compatibility with a hybrid GO model. J. Geophys. Res. Atmos. 112, D103104. http://dx.doi.org/10.1029/2006JD007445.
Myneni, R.B., Knyazikhin, Y., Privette, J.L., Glassy, J., Tian, Y., Wang, Y., et al., 2002. Global products of vegetation leaf area and fraction absorbed PAR from year one of MODIS data. Remote Sens. Environ. 83, 214–231.
Nasahara, K.N., Muraoka, H., Nagai, S., Mikami, H., 2008. Vertical integration of leaf area index in a Japanese deciduous broad-leaved forest. Agric. For. Meteorol. 148 (6–7), 1136–1146.
Nilson, T., 1971. A theoretical analysis of the frequency of gaps in plant stands. Agric. Meteorol. 8, 25–38.
Noormets, A., Gavazzi, M.J., Mcnulty, S.G., Domec, J.-C., Sun, G., King, J.S., Chen, J., 2010. Response of carbon fluxes to drought in a coastal plain loblolly pine forest. Glob. Chang. Biol. 16, 272–287.
Norman, J.M., 1982. Simulation of microclimates. In: Hatfield, J.L., Thomason, I.J. (Eds.), Biometeorology in Integrated Pest Management. Academic, San Diego, Calif, pp. 65–99.
Piayda, A., Dubbert, M., Werner, C., Vaz Correia, A., Pereira, J.S., Cuntz, M., 2015. Influence of woody tissue and leaf clumping on vertically resolved leaf area index and angular gap probability estimates. For. Ecol. Manag. 340, 103–113.
Pisek, J., Chen, J.M., Lacaze, R., Sonnentag, O., Alikas, K., 2010. Expanding global mapping of the foliage clumping index with multi-angular POLDER three measurements: evaluation and topographic compensation. ISPRS J. Photogramm. Remote Sens. 65, 341–346.
Pisek, J., Ryu, Y., Sprintsin, M., He, L., Oliphant, A.J., Korhonen, L., Kuusk, J., Kuusk, A., Bergstrom, R., Verrelst, J., 2013a. Retrieving vegetation clumping index from Multiangle Imaging SpectroRadiometer (MISR) data at 275 m resolution. Remote Sens. Environ. 138, 126–133.
Pisek, J., Sonnentag, O., Richardson, A., Mõttus, M., 2013b. Is the spherical leaf inclination angle distribution a valid assumption for temperate and borel broadleaf tree species. Agric. For. Meteorol. 169, 186–194.
Pisek, J., Govind, A., Arndt, S.K., Hocking, D., Wardlaw, T.J., Fang, H., Matteucci, G., Longdoz, B., 2015. Intercomparison of clumping index estimates from POLDER, MODIS, and MISR satellite data over reference sites. ISPRS J. Photogramm. Remote Sens. 101, 47–56.
Pueschel, P., Buddenbaum, H., Hill, J., 2012. An efficient approach to standardizing the processing of hemispherical images for the estimation of forest structural attributes. Agric. For. Meteorol. 160, 1–13.
Qu, Y., Meng, J., Wan, H., Li, Y., 2016. Preliminary study on integrated wireless smart terminals for leaf area index measurement. Comput. Electron. Agric. 129, 56–65.
Raabe, K., Pisek, J., Sonnentag, O., Annuk, K., 2015. Variations of leaf inclination angle distribution with height over the growing season and light exposure for eight broadleaf tree species. Agric. For. Meteorol. 214–215, 2–11.
Rambal, S., Ourcival, J.M., Joffre, R., Mouillot, F., Nouvellon, Y., Reichstein, M., Rocheteau, A., 2003. Drought controls over conductance and assimilation of a Mediterranean evergreen ecosystem: scaling from leaf to canopy. Glob. Chang. Biol. 9, 1813–1824.
Rautiainen, M., Mõttus, M., Stenberg, P., 2009. On the relationship of canopy LAI and photon recollision probability in boreal forests. Remote Sens. Environ. 113, 458–461.
Richardson, J.J., Moskal, L.M., Kim, S.-H., 2009. Modeling approaches to estimate effective leaf area index from aerial discrete-return LIDAR. Agric. For. Meteorol. 149 (6–7), 1152–1160.
Ross, J., 1981. The Radiation Regime and Architecture of Plant Stands. Junk Publishers, The Hague (391 pp.).
Ryu, Y., Nilson, T., Kobayashi, H., Sonnentag, O., Law, B.E., Baldocchi, D.D., 2010. On the correct estimation of effective leaf area index: does it reveal information on clumping effects? Agric. For. Meteorol. 150, 463–472.
Ryu, Y., Baldocchi, D.D., Kobayashi, H., Ingen, C., Li, J., Black, T.A., Beringer, J., Gorsel, E., Knohl, A., Law, B.E., 2011. Integration of MODIS land and atmosphere products with a coupled-process model to estimate gross primary productivity and evapotranspiration from 1 km to global scales. Glob. Biogeochem. Cycles 25, GB40117.
Schaaf, C.B., Gao, F., Strahler, A.H., Lucht, W., Li, X., Tsang, T., et al., 2002. First operational BRDF albedo, nadir reflectance products from MODIS. Remote Sens. Environ. 83, 135–148.
Serbin, S.P., Gower, S.T., Ahl, D.E., 2009. Canopy dynamics and phenology of a boreal black spruce wildfire chronosequence. Agric. For. Meteorol. 149, 187–204.
Shabanov, et al., 2003. Effect of foliage spatial heterogeneity in the MODIS LAI and FPAR algorithm over broadleaf forests. Remote Sens. Environ. 85, 410–423.
Smolander, S., Stenberg, P., 2005. Simple parameterizations of the radiation budget of uniform broadleaved and coniferous canopies. Remote Sens. Environ. 94, 355–363.
Solberg, S., Brunner, A., Hanssen, K.H., Lange, H., Næsset, E., Rautiainen, M., Stenberg, P., 2009. Mapping LAI in a Norway spruce forest using airborne laser scanning. Remote Sens. Environ. 113, 2317–2327.
Sonnentag, O., van der Kamp, G., Barr, A.G., Chen, J.M., 2010. On the relationship between water table depth and water vapor and carbon dioxide fluxes in a minerotrophic fen. Glob. Chang. Biol. 16, 1762–1776.
Sprintsin, M., Cohen, S., Maseyk, K., Rotenberg, E., Grunzweig, J., Karnieli, A., et al., 2011. Long term and seasonal courses of leaf area index in a semi-arid forest plantation. Agric. For. Meteorol. 151, 565–574.
Stenberg, P., 2007. Simple analytical formula for calculating average photon recollision probability in vegetation canopies. Remote Sens. Environ. 109, 221–224.
Stenberg, P., Kangas, T., Smolander, H., Linder, S., 1999. Shoot structure, canopy openness, and light interception in Norway spruce. Plant Cell Environ. 22, 1133–1142.
Stenberg, P., Palmroth, S., Bond, B., Sprugel, D., Smolander, H., 2001. Shoot structure and photosynthetic efficiency along the light gradient in a Scots pine canopy. Tree Physiol. 21, 805–814.
Stenberg, P., Mõttus, M., Rautiainen, M., 2016. Photon recollision probability in modelling the radiation regime of canopies—a review. Remote Sens. Environ. 183, 98–108.
Talbot, J., Roulet, N.T., Sonnentag, O., Moore, T.R., 2014. Increases in aboveground biomass and leaf area 85 years after drainage in a bog. Botany 92, 713–721.
Tanaka, N., Kume, T., Yoshifuji, N., Tanaka, K., Takizawa, H., Shiraki, K., Tantasirin, C., Tangtham, N., Suzuki, M., 2008. A review of evapotranspiration estimates from tropical forests in Thailand and adjacent regions. Agric. For. Meteorol. 148, 807–819.
Taugourdeau, S., le Maire, G., Avelino, J., Jones, J.R., Ramirez, L.G., Jara Quesada, M., ... Roupsard, O., 2014. Leaf area index as an indicator of ecosystem services and management practices: an application for coffee agroforestry. Agric. Ecosyst. Environ. 192, 19–37.
Tedeschi, V., Rey, A., Manca, G., Valentini, R., Jarvis, P.G., Borghetti, M., 2006. Soil respiration in a Mediterranean oak forest at different developmental stages after coppicing. Glob. Chang. Biol. 12, 110–121.
Thimonier, A., Sedivy, I., Schleppi, P., 2010. Estimating leaf area index in different types of mature forest stands in Switzerland: a comparison of methods. Eur. J. For. Res. 129, 543–562.
Urbanski, S., Barford, C., Wofsy, S., Kucharik, C., Pyle, E., Budney, J., McKain, K., Fitzjarrald, D., Czikowsky, M., Munger, J.W., 2007. Factors controlling CO_2 exchange on timescales from hourly to decadal at Harvard Forest. Journal of Geophysical Research-Biogeosciences 112 (G02020). http://dx.doi.org/10.1029/2006JG000293.
Verger, A., Martínez, B., Coca, F.C.D., García-Haro, F.J., 2009. Accuracy assessment of fraction of vegetation cover and leaf area index estimates from pragmatic methods in a cropland area. Int. J. Remote Sens. 30, 2685–2704.
Vuolo, F., Neugebauer, N., Bolognesi, S.F., Atzberger, C., D'Urso, G., 2013. Estimation of leaf area index using DEIMOS-1 data: application and transferability of a semi-empirical relationship between two agricultural areas. Remote Sens. 5, 1274–1291.
Wei, S., Fang, H., 2016. Estimation of canopy clumping index from MISR and MODIS sensors using the normalized difference hotspot and darkspot (NDHD) method: the influence of BRDF models and solar zenith angle. Remote Sens. Environ. 187, 476–491.
Yan, K., Park, T., Yan, G., Chen, C., Yang, B., Liu, Z., Nemani, R., Knyazikhin, Y., Myneni, R., 2016a. Evaluation of MODIS LAI/FPAR product collection 6. Part 1: consistency and improvements. Remote Sens. 8, 359.
Yan, K., Park, T., Yan, G., Liu, Z., Yang, B., Chen, C., Nemani, R., Knyazikhin, Y., Myneni, R., 2016b. Evaluation of MODIS LAI/FPAR product collection 6. Part 2: validation and intercomparison. Remote Sens. 8, 460.